Supplemental Information: Air Quality Impact and Physicochemical Aging of Biomass Burning Aerosols during the 2007 San Diego Wildfires

Melanie D. Zauscher,[a] Ying Wang,[b] Meagan J.K. Moore,[a] Cassandra J. Gaston,[c] and Kimberly A. Prather[b,c,]*

[a]Department of Mechanical and Aerospace Engineering, University of California, San Diego

[b]Department of Chemistry and Biochemistry, University of California, San Diego

[c]Scripps Institution of Oceanography, University of California, San Diego

* To whom correspondence should be addressed, email: kprather@ucsd.edu, fax 858-534-7042

This supporting information contains 6 sections, listed below, on 19 pages with 10 figures:

1. ATOFMS data analysis
2. Positive matrix factorization analysis
3. Biomass burning aerosol particle types
4. Organic acid standards
5. Gas phase data
6. Insights from chemical markers

18

1. ATOFMS data analysis

20 Parameters used in ART-2a analysis were: vigilance factor of 0.85, learning rate of 0.05
21 and iteration number of 20. The most intense peak in BBA is from the potassium ion, $^{39}K^+$.
22 Although the +39 m/z could also the $^{39}C_3H_3^+$ organic marker, the majority of it is likely to be
23 from $^{39}K^+$ due to its high ionization potential and known large emissions during biomass
24 burning.[1-3]

25 As particle size increases, there is a smaller contribution of BBA particles. At 300 nm,
26 over 60% of the particles were classified as BBA, while at 400 nm only about 40% of particles
27 were identified as BBA. Particles with diameters > 400 nm tended to be of vehicular traffic
28 origin, but extensively atmospherically processed with amines; ~25% and ~60% of particles at
29 400 nm and 1000 nm were aged vehicular traffic particles. Up to 15% of particles were sea salt
30 particles. Because the goal of this study was to characterize BBA particles, the analysis of the
31 data reported was for particles with diameters < 400 nm.

2. Positive matrix factorization analysis

33 The PMF model used was the USEPA PMF 3.0. The guidelines presented in the
34 Fundamentals & User Guide were followed during the analysis.[4] However, instead of using PMF
35 for determining the source of aerosols, we used PMF in this study to group chemical markers
36 from particles of the same source, namely biomass burning. The signal-to-noise ratio of all
37 species used in PMF analysis was > 1 indicating that the variability in the measurements was real
38 and therefore all 19 marker species were categorized as strong in the PMF model.[4] In 956 fifteen
39 minute samples, there was only one missing value across all species on 10/26/07 9:00, which
40 was replaced with the geometric mean value of the preceding and following 3 hours of the
41 missing value for each species. The PMF base model was set-up with a random seed and 100
42 runs, which all converged.

43 Solutions for 3-13 factors were considered and the relevant Q values for each of these
44 cases are shown in Table S1. In all solutions explored $Q_{theory} > Q_{robust}$, although it is
45 recommended that $Q_{theory} \approx Q_{robust}$.[4] The 3-factor solution had the closest Q_{theory} to Q_{robust}, but the

three factors were inadequate in describing the temporal variability of the species. As the number of factors increased, Q_{robust} decreased at a faster rate than Q_{theory} (EPA2.0). On the other hand, the predicted species better matched the observed species in time as the number of factors was increased. Because the correlations between observed and predicted variables were strong (R^2> 0.85), the residuals were between -2 and 2, and the resulting factors made physical sense,[5] we chose the 10-factor PMF solution as the final one. The 9-factor solution had less strong correlations between observed and predicted species; specifically $^{26}CN^-$ and $^{89}HC_2O_4^-$ markers had R^2 < 0.85. There was no potassium nitrate factor in the 9-factor solution. The 11-factor solution, with slightly stronger R^2 values (R^2 > 0.88) than the 10-factor solution, had two organic nitrogen factors, which seemed less physically meaningful. These observations led us to choose the 10-factor solution as the final solution, even though $Q_{robust} << Q_{theory}$, despite the recommendation that $Q_{theory} \approx Q_{robust}$. Bootstrapping was performed to check the stability of the solution. Furthermore, G-space was used to investigate rotational ambiguity in the factor solutions by varying F_{peak} between -0.5-0.5.[6] For the chosen 10-factor solution, Q_{theory}= 8414 using the PMF2.0 definition.[4,7] The 10-factor solution with F_{peak}=0 had $Q_{robust}=Q_{true}$=658. The solution which removed the oblique edges between every pair of factors was for F_{peak} = -0.2 and is presented herein thus, changing the Q values to Q_{true}=671.0 and Q_{robust}=1698.2.

3. Biomass burning aerosol particle types

Figure S6 shows the mass spectra for the five biomass burning aerosols (BBA) observed during this study: BBA-sulfate-nitrate, BBA-nitrate-sulfate, BBA-soot, BBA-soot-sulfate-nitrate, and BBA-OC-sulfate-nitrate. The BBA-sulfate-nitrate particle type, where the $^{97}HSO_4^-$ ion peak intensity was slightly greater than that of $^{62}NO_3^-$, was present throughout the study and represented 91% of all BBA. The BBA-nitrate-sulfate particle type, which contained more intense $^{62}NO_3^-$ than $^{97}HSO_4^-$ peaks, contributed 6% to all BBA by number. As shown in Figure 1, BBA-nitrate-sulfate peaked in the day probably due to the photochemical formation of nitrate. The BBA-soot particle type, which only contributed ~1% to all BBA numbers, had moderately intense $^{12n}C_n^+$ peaks, and was more prevalent during the last 3 days of the study. Perhaps, during this time there was coagulation and cloud processing of BBA with combustion particles from the LA and LB ports and Riverside. The lack of negative mass spectra in the BBA-soot particle type supports that these were wet, and thus aged particles.[8] The BBA-soot-sulfate-nitrate had similar

positive mass spectra as the BBA-soot type, but with peaks at $^{97}HSO_4^-$ and $^{62}NO_3^-$. The BBA-OC-sulfate-nitrate particle type had moderately intense OC peaks, such as $^{27}C_2H_3^+$ and $^{43}C_2H_3O^+$, with a very intense $^{97}HSO_4^-$ peak. The BBA-OC-sulfate-nitrate and the BBA-soot-sulfate-nitrate particle type made up only 0.6 and 0.4% of all BBA particles, respectively. Previous single particle aerosol mass spectrometer studies have also identified different BBA particle types during ambient measurements.[9,10]

In this study, BBA were internally mixed with either $^{62}NO_3^-$ or $^{97}HSO_4^-$, both acidic species, in roughly equal percentages by number (82 versus 80%), within or similar to the range of previous observations (21-100% and 92-100%, respectively).[11,12] Furthermore, 73% of BBA by number had both $^{97}HSO_4^-$ and $^{62}NO_3^-$ internally mixed together. The occurrence of the $^{125}HNO_3NO_3^-$ peak, which may indicate the presence of nitric acid, was found on almost half of the BBA sampled and was more intense on 10/25/07 coincident with increased RH, and spike in $^{62}NO_3^-$. Previous studies have observed 21-59% of BBA number fraction internally mixed with $^{125}HNO_3NO_3^-$.[12] 69% of BBA were internally mixed with oxalate, a weak acid, in contrast with 28-94% in previous studies.[11-13] $^{18}NH_4^+$, which is basic, was found on 76% of BBA particle numbers, whereas previous studies have only detected $^{18}NH_4^+$ internally mixed in 8-58% of BBA.[11,12] In addition, 76% of BBA were internally mixed with amines, also basic, based on the presence of the $^{86}(C_2H_5)_2NCH_2^+$ fragment.[14] Potassium salts were prevalent in most BBA with > 50, 60 and 70% of BBA having $^{140}K_2NO_3^+$, $^{113}K_2Cl^+$, and $^{213}K_3SO_4^+$, respectively. Potassium salts were found to be internally mixed together in 43, 52 and 49% of BBA as $^{113}K_2Cl^+$ and $^{140}K_2NO_3^+$, $^{113}K_2Cl^+$ and $^{213}K_3SO_4^+$, and $^{140}K_2NO_3^+$ and $^{213}K_3SO_4^+$, respectively; 36% of BBA had all three potassium salts internally mixed. The percentages of BBA internally mixed with all these species depend on fire conditions, regionally background pollutant levels, and meteorology.

4. Organic acid standards

Solutions of sodium pyruvate (Fisher), sodium glycolate (Acros), sodium propanoate (Spectrum), glyoxylic acid (Acros), methylglyoxal (Sigma), zinc acrylate (Aldrich), in addition to levoglucosan (Acros), were made with ultra-pure water and atomized to generate particles. The particles were dried downstream with diffusion dryers before entering the ATOFMS inlet. At least 2,000 mass spectra were obtained per standard for statistical significance. A

representative negative mass spectrum for each standard is shown in Figure S8. The pyruvate, glycolate and glyoxylate generated molecular ions at -87, -75, and -73 m/z, respectively, whereas the molecular ion from methylglyoxal and acrylate was at -71 m/z. Most standards also had small peaks at -59 and -45 m/z in their mass spectra. Because ions from different standards known to be present in BBA were formed at -71 and -73 m/z, it is not possible to attribute these peaks to a specific compound. Thus, in addition to levoglucosan fragments, the peaks at -71, -73, -75, and -87 m/z could be the resulting ions of several organic acids.

5. Gas phase data

Figure S9 shows the gas phase concentrations measured at Escondido and San Diego California Air Resources Board (CARB) sites from 10/11/07 until 11/01/07. Overall, the NO_x was higher at San Diego site compared to Escondido. The concentrations of nitrogen oxides (NO_x) exceeded the 1-hour National Ambient Air Quality Standard (NAAQS) standard (0.1 ppm) during a few periods between 10/23/07-10/25/07. The highest NO_x reported was 0.37 ppm at the San Diego site at 10/24/07 8:00 compared to 0.21 ppm at Escondido an hour before. It is interesting that the NOx concentrations were higher at the San Diego site than at Escondido during the 12 days after the first wildfire, with an average of 0.07 ± 0.06 versus 0.05 ± 0.04 ppm, respectively. The 10 days preceding the wildfires, the NOx concentrations were 0.03 ± 0.04 and 0.02 ± 0.02 ppm at San Diego and Escondido, respectively. There was no statistically significant difference (using p-test) for the daily profiles of O_3 before and after the wildfires started. At the beginning of the wildfires (10/21/07 morning thru the afternoon of 10/23/07), O_3 remained high at Escondido, but the rest of the time the O_3 was typical of a non-fires period with a strong diurnal pattern. A modeling study showed that the O_3 from the 2007 California wildfires peaked over the ocean because by the time the precursors generated O_3 the winds had blown the air mass offshore.[15] Carbon monoxide (CO) concentrations were fairly low overall, but roughly twice as high from 10/11/07-10/20/07 compared to 10/21/07-11/1/07.

The amount of nitrogen present in the fuel and the type of fire determines how much $NO_{x(g)}$ and $NH_{3(g)}$ are formed.[16] $NO_{x(g)}$ and $NH_{3(g)}$ preferentially form during flaming and smoldering conditions, respectively.[17] Unfortunately, we cannot compare $NH_{3(g)}$ to $NO_{x(g)}$ because $NH_{3(g)}$ was not measured during the 2007 San Diego wildfires. Both $NO_{x(g)}$ and $NH_{3(g)}$ may eventually partition into the particle phase as $^{62}NO_3^-$ and $^{18}NH_4^+$, respectively. Another gas

species of interest is $SO_{2(g)}$, which can oxidize into $H_2SO_{4(g)}$ and eventually partition into the particle phase as SO_4^{2-}. Although there is some $SO_{2(g)}$ emitted from biomass burning, previous studies found it less significant than the emitted $NO_{x(g)}$.[17-20] In San Diego County, only the San Diego CARB site measured the concentration of $SO_{2(g)}$ and it was low and stable during this study, indicating that either biomass burning in Southern California does not generate substantial emissions of $SO_{2(g)}$ or that it reacts very quickly. Interestingly, $NO_{x(g)}$ and $CO_{(g)}$ peaked in the morning and then at night on 10/23/07-10/26/07. The night-time peak was probably due to a lower nocturnal boundary layer, whereas the morning peak was likely a result of photochemistry. The hypothesized low nocturnal boundary layer would trap the wildfire emissions from diluting and mixing with the rest of the troposphere and hence concentrate the emissions.

6. Insights from Chemical Markers

Figure S10 shows the mixing state of $^{18}NH_4^+$, $^{62}NO_3^-$, $^{97}HSO_4^-$ and $^{89}HC_2O_4^-$ on individual BBA particles during two different periods. In each ternary plot, BBA containing mostly nitrate would be towards the right vertex, mostly sulfate towards the top vertex, and mostly oxalate towards the left vertex; the color represents different amounts of ammonium. Each ternary plot represents a different period chosen to represent different conditions, the beginning of the fires (10/22/07 12:00 – 10/23/07 17:53) and a period when nitric acid spiked (10/25/07 12:00 – 10/26/07 12:00). The number of BBA from the beginning of the fires was cut-off at 99,999 in order to make the amount of data manageable for the ternary plot. During the beginning of the fires, there was a greater distribution in the mixing state of BBA compared with the nitric acid spike period. At the beginning of the fires, there were particles with mostly oxalate, mostly sulfate, mostly nitrate, and particles internally mixed with different amounts of all three species. During the high nitric acid period, the majority of particles had significant amounts of nitrate, little oxalate and a broad distribution of sulfate. The distribution of ammonium was also different during both periods. In the beginning of the fires, higher amounts of $^{18}NH_4^+$ were predominantly associated with sulfate only BBA indicating that during this period, and most of the fires (not shown), ammonium was predominantly found as $(NH_4)_2SO_4$ and not NH_4NO_3. During the nitric acid spike, higher amounts of $^{18}NH_4^+$ were mostly associated with nitrate. Because sulfuric acid is a stronger acid than nitric acid, there must not have been enough sulfuric acid to neutralize the

ammonium during this period. Thus, during the nitric acid spike, there was a prevalence of NH_4NO_3 over $(NH_4)_2SO_4$, which has been observed before in BBA.[19,20]

It is also worth noting the differences in the nitrate markers across different nitrogen factors. Through PMF analysis, 49, 38, 4, and 0% of the $^{62}NO_3^-$ was assigned to the *nitrate factor*, *ammonium nitrate factor*, *potassium nitrate factor*, and *organic nitrogen factor*, respectively. In contrast, 58, 18, 11, and 0% of the $^{46}NO_2^-$ were in the *nitrate factor*, *organic nitrogen factor*, *ammonium nitrate factor*, and *potassium nitrate factor*, respectively. Finally, 53 and 12% of the $^{125}HNO_3NO_3^-$ were found in the *ammonium nitrate factor* and *potassium nitrate factor*, while no $^{125}HNO_3NO_3^-$ was associated with the *nitrate factor* or *organic nitrogen factor*. At high temperatures, refractory material is stable, whereas non-refractory material is not. KNO_3 and NH_4NO_3 are examples of refractory and non-refractory nitrate, respectively. It is worth noting that the *nitrate factor* had the highest contribution of $^{140}K_2NO_3^+$ (38%), with the *potassium nitrate factor* having the second most amount of $^{140}K_2NO_3^+$ (33%); thus, both the *nitrate factor* and *potassium nitrate factor* were indicative of refractory nitrate. Based on the prevalence of $^{125}HNO_3NO_3^-$ in the *ammonium nitrate factor* compared to $^{62}NO_3^-$ and $^{46}NO_2^-$, it can be concluded that $^{125}HNO_3NO_3^-$ represents mostly non-refractory nitrate while $^{62}NO_3^-$ and $^{46}NO_2^-$ were present in both refractory and non-refractory nitrate. Furthermore, these observations indicate that a small percentage of $^{46}NO_2^-$ (18%) was also formed from organic nitrogen species, while $^{62}NO_3^-$ and $^{125}HNO_3NO_3^-$ were not.

189

Table S1: Q values for PMF Analysis with different number of factors. $^{*}Q_{robust}$ with $F_{peak} = 0$

# of Factors	R^2 between observed and predicted species	Q_{robust} *	Q_{theory} (EPA2.0)
3	0.00-0.92	5254	15329
4	0.49-0.92	3314	14264
5	0.53-0.95	2506	13289
6	0.68-0.97	1824	12314
7	0.68-0.99	1388	11339
8	0.72-0.99	1034	10364
9	0.78-0.99	834	9389
10	0.85-0.99	658	8414
11	0.88-0.99	532	7439
12	0.93-0.99	418	6464
13	0.95-0.99	316	5489

190

191

192

193

194

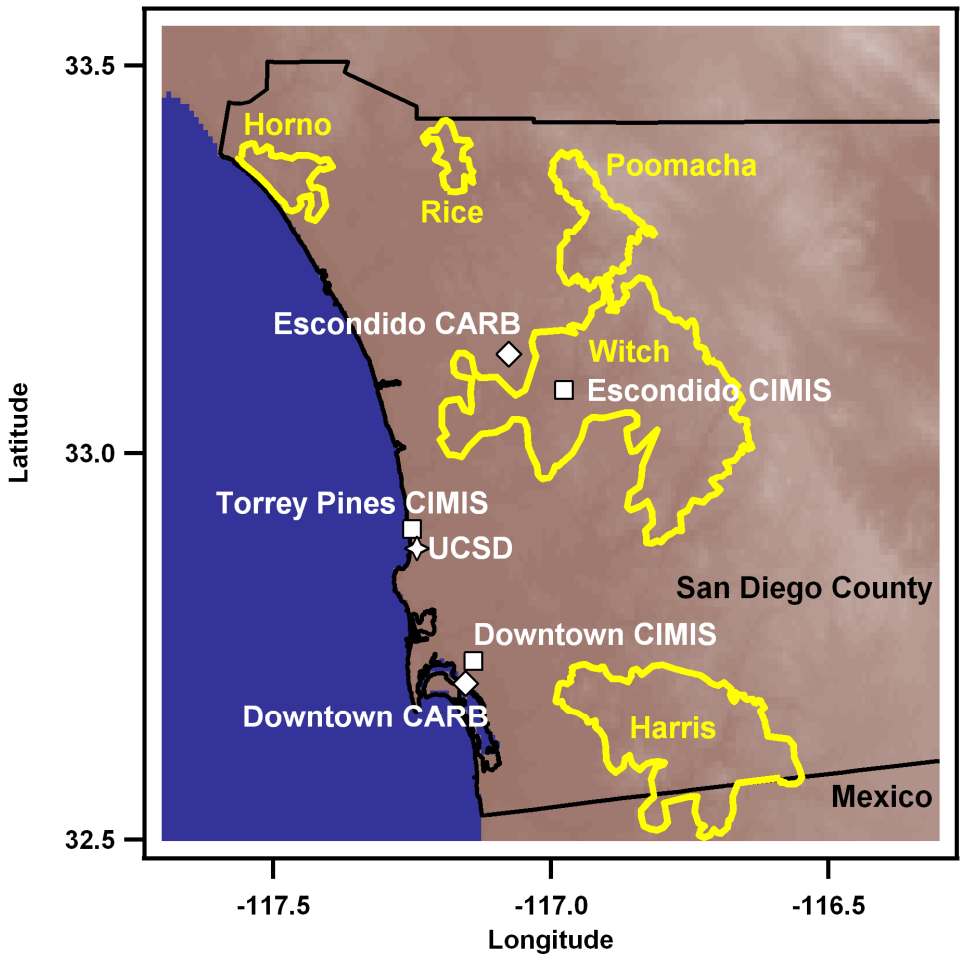

Figure S1: Map of wildfire perimeters in San Diego County, October, 2007 and sampling sites. Aerosol physicochemical properties were measured at the University of California San Diego (UCSD). Gas phase and particulate matter 2.5 µm ($PM_{2.5}$) mass concentrations were obtained from the California Air Resources Board (CARB) while meteorological data was obtained from the California Irrigation Management Information System (CIMIS), respectively.

195

196

197

198

199

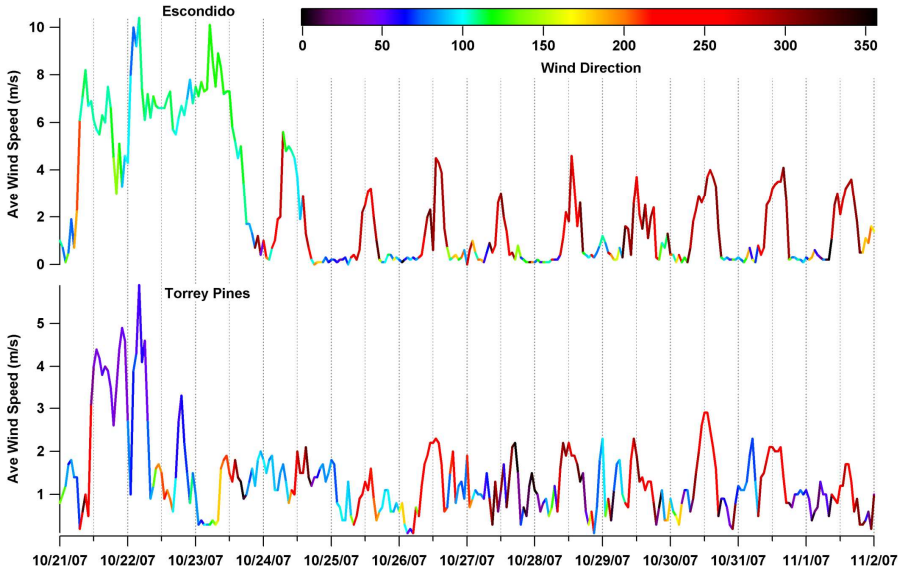

Figure S2: Wind Patterns from Escondido and Torrey Pines sites collected through the CIMIS network.

200

201

202

203

204

205

206

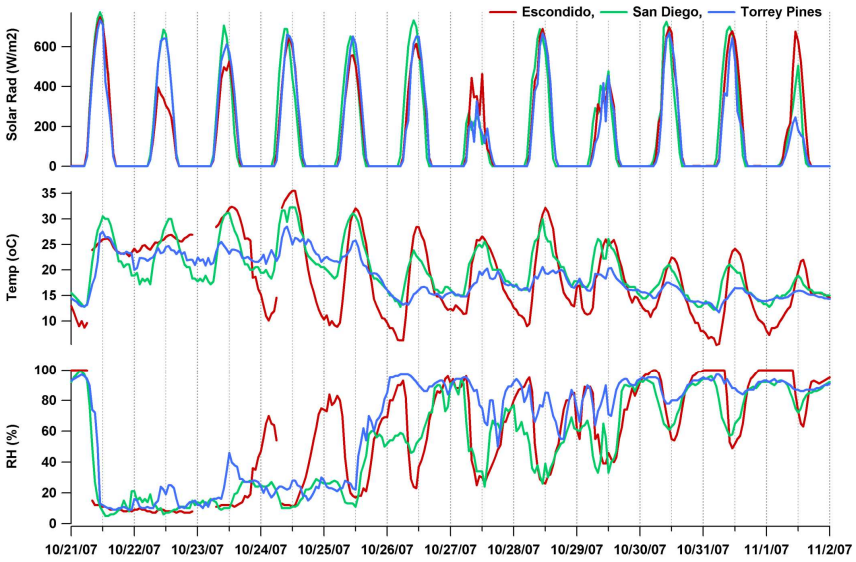

Figure S3: Meteorological data from Escondido, San Diego and Torrey Pines sites collected through the CIMIS network.

207

208

209

Figure S4: MODIS image from 10/23/10 11:45. Red dots indicate active fires.

210

211

212

213

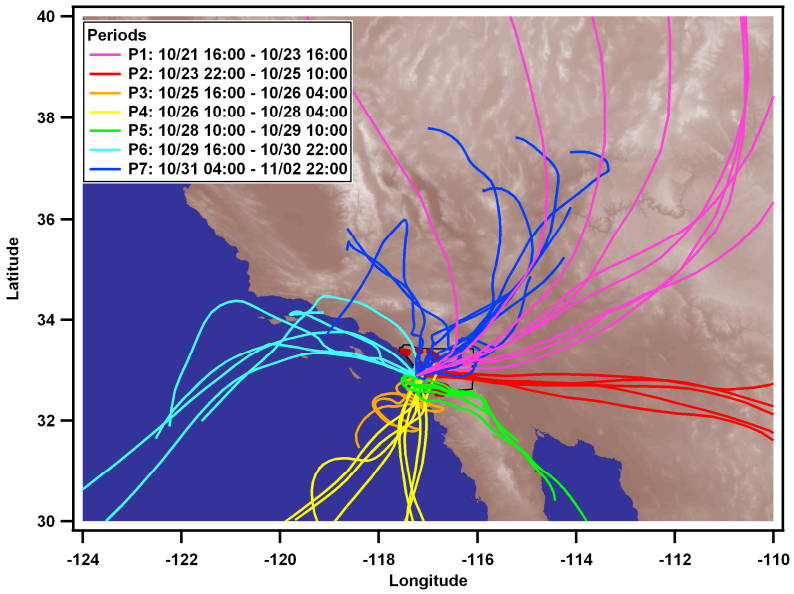

Figure S5: Air mass back trajectories during study determined using HYSPLIT at 500 m altitude.

214

215

216

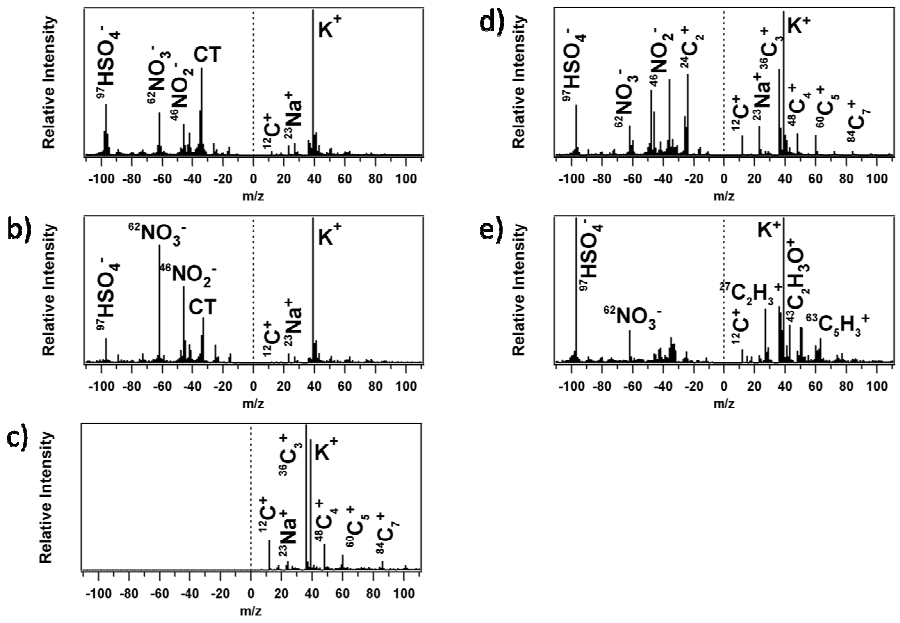

Figure S6: Mass spectra of the different types of 100-400nm particles types detected during 2007 San Diego Wildfires: a) BBA-sulfate-nitrate, b) BBA-nitrate-sulfate, c) BBA-soot, d) BBA-soot-sulfate-nitrate, and e) BBA-OC-sulfate-nitrate. CT refers to cross talk interference.

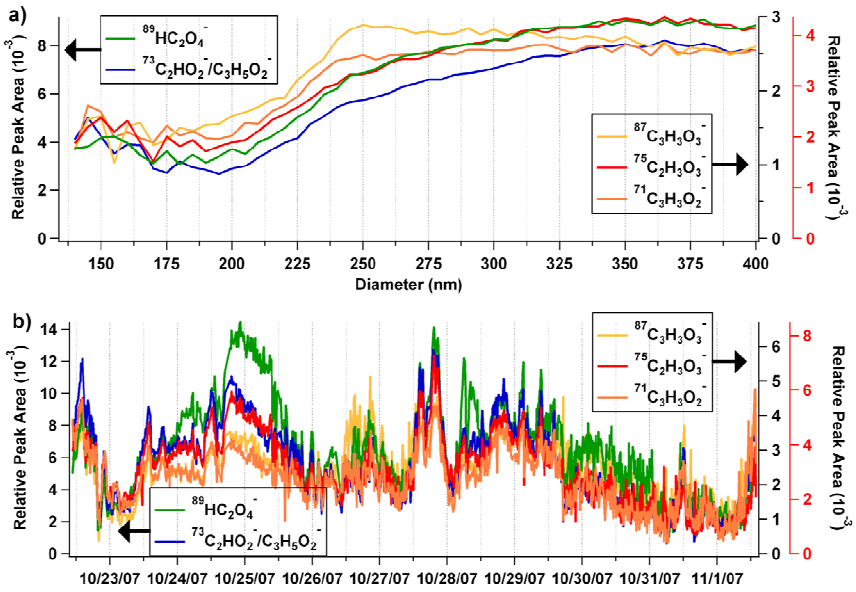

Figure S7: Distributions of the relative peak areas of organic acids in BBA by a) particle size and b) time.

232

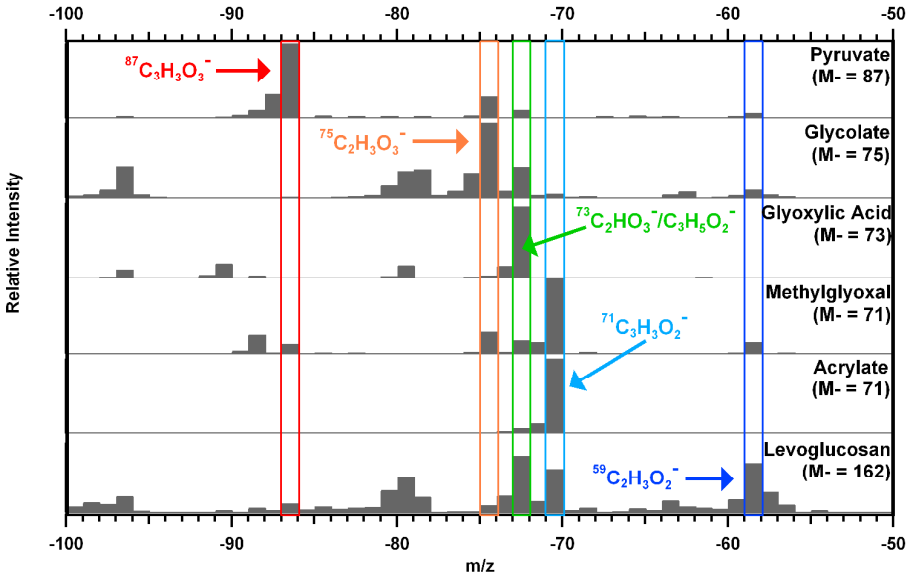

Figure S8: Mass spectra of organic acid standards averaged over 2000 particles.

233

234

235

236

237

238

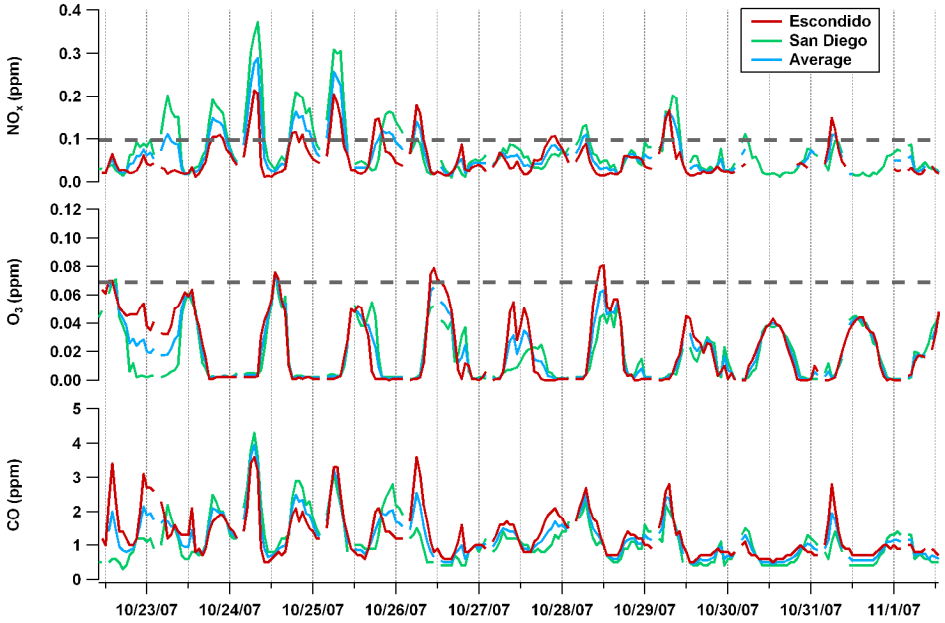

Figure S9: Gas phase concentrations. Dashed lines indicate 24-hour National Ambient Air Quality Standard. Data collected from CARB.

239

240

241

242

243

244

245

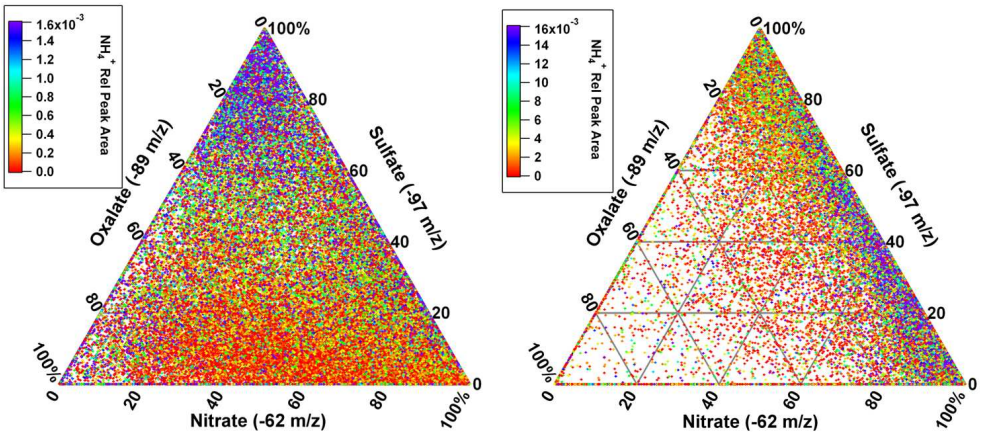

Figure S10: Ternary plots show the mixing state of ammonium, sulfate, nitrate, and oxalate in 100-400 nm BBA during a) the beginning of the fires (10/22/07 10:00-10/23/07 17:53) and b) during spike in nitric acid (10/25/07 12:00 - 10/26/07 12:00). There were 99,999 and 69,255 particles during each period, respectively. Each point on the plots represents a single particle.

References

(1) Andreae, M. O. *Science* **1983**, *220*, 1148-1151.

(2) Gross, D. S.; Galli, M. E.; Silva, P. J.; Prather, K. A. *Analytical Chemistry* **2000**, *72*, 416-422.

(3) Silva, P. J.; Liu, D.; Noble, C. A.; Prather, K. A. *Environmental Science & Technology* **1999**, *33*, 3068-3076.

(4) Autho; USEPA Office of Research and Development, 2008.

(5) Reff, A.; Eberly, S. I.; Bhave, P. V. *Journal of the Air & Waste Management Association* **2007**, *57*, 146-154.

(6) Paatero, P.; Hopke, P. K.; Begum, B. A.; Biswas, S. K. *Atmospheric Environment* **2005**, *39*, 193-201.

(7) Chan, Y. C.; Hawas, O.; Hawker, D.; Vowles, P.; Cohen, D. D.; Stelcer, E.; Simpson, R.; Golding, G.; Christensen, E. *Atmospheric Environment* **2011**, *45*, 439-449.

(8) Neubauer, K. R.; Johnston, M. V.; Wexler, A. S. *Atmospheric Environment* **1998**, *32*, 2521-2529.

(9) Bi, X. H.; Zhang, G. H.; Li, L.; Wang, X. M.; Li, M.; Sheng, G. Y.; Fu, J. M.; Zhou, Z. *Atmospheric Environment* **2011**, *45*, 3447-3453.

(10) McGuire, M. L.; Jeong, C. H.; Slowik, J. G.; Chang, R. Y. W.; Corbin, J. C.; Lu, G.; Mihele, C.; Rehbein, P. J. G.; Sills, D. M. L.; Abbatt, J. P. D.; Brook, J. R.; Evans, G. J. *Atmospheric Chemistry and Physics* **2011**, *11*, 8133-8155.

(11) Pratt, K. A.; Heymsfield, A. J.; Twohy, C. H.; Murphy, S. M.; DeMott, P. J.; Hudson, J. G.; Subramanian, R.; Wang, Z. E.; Seinfeld, J. H.; Prather, K. A. *Journal of the Atmospheric Sciences* **2010**, *67*, 2451-2468.

(12) Pratt, K. A.; Murphy, S. M.; Subramanian, R.; DeMott, P. J.; Kok, G. L.; Campos, T.; Rogers, D. C.; Prenni, A. J.; Heymsfield, A. J.; Seinfeld, J. H.; Prather, K. A. *Atmospheric Chemistry and Physics* **2011**, *11*, 12549-12565.

(13) Moffet, R. C.; de Foy, B.; Molina, L. T.; Molina, M. J.; Prather, K. A. *Atmospheric Chemistry and Physics* **2008**, *8*, 4499-4516.

(14) Angelino, S.; Suess, D. T.; Prather, K. A. *Environmental Science & Technology* **2001**, *35*, 3130-3138.

(15) Pfister, G. G.; Wiedinmyer, C.; Emmons, L. K. *Geophysical Research Letters* **2008**, *35*, 5.

(16) Reid, J. S.; Koppmann, R.; Eck, T. F.; Eleuterio, D. P. *Atmospheric Chemistry and Physics* **2005**, *5*, 799-825.

(17) Andreae, M. O.; Merlet, P. *Global Biogeochemical Cycles* **2001**, *15*, 955-966.

(18) Streets, D. G.; Yarber, K. F.; Woo, J. H.; Carmichael, G. R. *Global Biogeochemical Cycles* **2003**, *17*, 20.

(19) Fiedler, V.; Arnold, F.; Ludmann, S.; Minikin, A.; Hamburger, T.; Pirjola, L.; Dornbrack, A.; Schlager, H. *Atmospheric Chemistry and Physics* **2011**, *11*, 3211-3225.

(20) Song, C. H.; Ma, Y.; Orsini, D.; Kim, Y. P.; Weber, R. J. *Journal of Atmospheric Chemistry* **2005**, *51*, 43-64.